Liquid Crystals
Publication details, including instructions for authors and subscription information:
http://www.informaworld.com/smpp/title~content=t713926090

Laterally substituted naphthalene-2,7-diol-based bent-shaped liquid crystals

Václav Kozmík[a]; Martin Kuchař[a]; Jiří Svoboda[a]; Vladimíra Novotná[b]; Milada Glogarová[b]; Ute Baumeister[c]; Siegmar Diele[c]; Gerhard Pelzl[c]
[a] Department of Organic Chemistry, Institute of Chemical Technology, CZ-166 28 Prague 6, Czech Republic [b] Institute of Physics, Academy of Sciences of the Czech Republic, CZ-180 40 Prague 8, Czech Republic [c] Institut für Physikalische Chemie, Martin-Luther-Universität Halle-Wittenberg, D-06106 Halle, Germany

To cite this Article Kozmík, Václav , Kuchař, Martin , Svoboda, Jiří , Novotná, Vladimíra , Glogarová, Milada , Baumeister, Ute , Diele, Siegmar and Pelzl, Gerhard(2005) 'Laterally substituted naphthalene-2,7-diol-based bent-shaped liquid crystals', Liquid Crystals, 32: 9, 1151 — 1160
To link to this Article: DOI: 10.1080/02678290500284231
URL: http://dx.doi.org/10.1080/02678290500284231

Liquid Crystals, Vol. 32, No. 9, September 2005, 1151–1160

Laterally substituted naphthalene-2,7-diol-based bent-shaped liquid crystals

VÁCLAV KOZMÍK†, MARTIN KUCHAŘ†, JIŘÍ SVOBODA*†, VLADIMÍRA NOVOTNÁ‡, MILADA GLOGAROVÁ‡, UTE BAUMEISTER§, SIEGMAR DIELE§ and GERHARD PELZL§

†Department of Organic Chemistry, Institute of Chemical Technology, Technická 5, CZ-166 28 Prague 6, Czech Republic

‡Institute of Physics, Academy of Sciences of the Czech Republic, Na Slovance 2, CZ-180 40 Prague 8, Czech Republic

§Institut für Physikalische Chemie, Martin-Luther-Universität Halle-Wittenberg, Mühlpforte 1, D-06106 Halle, Germany

(*Received 18 February 2005; accepted 16 May 2005*)

Novel series of laterally 1-substitued (H, Cl, CH_3, CN, NO_2) naphthalene-2,7-diol based liquid crystals were synthesized and their mesomorphic properties identified using DSC studies, texture observation, X-ray investigations and electro-optical measurements. Depending on the chain length and type of lateral substitution, the compounds exhibit a variety of mesophases. In materials with short alkyl chains, the rectangular columnar B_1 phase was found. Increasing the alkyl chain length for the non-substituted core causes the appearance of the so-called B_N phase. In CH_3- and Cl-substituted compounds, the antiferroelectric B_2 phase (SmC_AP_A) was found. Introduction of the CN and NO_2 substituents led to the formation of the B_7 phase.

1. Introduction

Bent-shaped liquid crystals represent a new sub-field of thermotropic liquid crystals. They have attracted considerable interest as they may exhibit polar smectic phases [1]. In recent years a great number of such compounds have been synthesized and their mesomorphic behaviour investigated [2–21]. The majority of bent-shaped mesogens are based on a 1,3-phenylene unit in the central core. It was found that lateral substitution in the core and in the outer rings influences the formation and type of mesophases. Structure–property relationships of banana-shaped mesogens have also recently been summarized [3, 12, 13], however, these relationships are not yet completely understood.

A limited number of compounds possessing the naphthalene-2,7-diol system in the core have been described [3, 22]. Recently, Sadashiva *et al.* [23–26] studied the mesomorphic properties of various symmetrical and unsymmetrical bent-shaped mesogens based on this core and characterized their mesomorphic properties. In the meantime we studied [27] the synthesis and mesomorphic behaviour of a series of Schiff's bases derived from laterally 1-substituted naphthalene-2,7-diol and found a strong dependence of the type of the B phase formed on the nature of the lateral substituent. However, high transition temperatures and rather low thermal and electric field stability of some of these compounds prevented their complete investigation. In this paper we report the synthesis and physical study of new series of laterally substituted napthalene-2,7-diol-based materials, in which the imine unit was replaced by an ester moiety, leading to more stable materials with lower transition temperatures. The mesomorphic properties of 20 newly synthesized compounds have been studied and investigated.

2. Experimental

2.1. *Characterization*

The molecular structure of the synthesized compounds was confirmed by spectroscopic methods. ^{1}H NMR spectra were obtained on Varian-Gemini 300 HC spectrometers. Deuteriochloroform and DMSO-d_6 served as solvents, and the signals of the solvent were used as internal standards. Chemical shifts are reported in the δ-scale (ppm), coupling constants J(H,H) in Hz. Infrared (IR) spectra were recorded on a Nicolet FTIR 740 spectrometer in KBr pellets.

*Corresponding author. Email: Jiri.Svoboda@vscht.cz

Liquid Crystals
ISSN 0267-8292 print/ISSN 1366-5855 online © 2005 Taylor & Francis
http://www.tandf.co.uk/journals
DOI: 10.1080/02678290500284231

The phase transition temperatures and enthalpies were determined by DSC studies (Pyris Diamond Perkin-Elmer 7) under cooling and heating runs at a rate of 5 K min^{-1}. The 2–5 mg samples were placed in a nitrogen atmosphere and hermetically sealed in aluminium pans.

Mesophase identification was based on microscopic examination of textures in both planar and free-standing films, switching and dielectric properties and X-ray studies. A Nikon polarizing microscope equipped with a Linkam hot stage was used. The memory oscilloscope leCroy 9304 provided the switching characteristics. The measurement of the frequency dispersion of permittivity was performed on cooling using a Schlumberger 1260 impedance analyser in the frequency range 1 Hz–1 MHz, keeping the temperature of the sample stable during sweeps within ± 0.1 K.

The planar samples for texture and electric field studies were composed of glass plates with ITO transparent electrodes ($5 \times 5\,mm^2$) and filled by capillarity action in the isotropic phase. The sample thickness was defined by mylar sheets usually as 6 µm. X-ray measurements were carried out on powder samples using a Guiner camera. To evaluate the molecular length a simulation of the CPK model was used.

2.2. *Synthesis*

The syntheses of the central 1-substituted naphthalene-2,7-diols (**1b**–**d**) have been described previously [27]. The nitro derivative **1e** was obtained from 2,7-dimethoxynaphthalene by a modified route [28, 29]. 2,7-Dimethoxynaphthalene was first nitrated with concentrated nitric acid. Deprotection of the methyl groups in the 1-nitroderivative formed was achieved by heating with pyridinium chloride at 170°C. Unlike the published multistep synthesis of related materials [25], the target materials **3** were simply obtained by a one-step standard DCC coupling procedure of **1a**–**e** with the known 4-[(4-alkoxybenzoyl)oxy]benzoic acids (**2**$_n$) in the presence of DMAP (see scheme 1). The acids **2**$_n$ were obtained by a known procedure [30]. Only new synthetic procedures are described in detail.

2.2.1. 1-Nitro-2,7-dimethoxynapthalene. To a solution of 2,7-dimethoxynapthalene (20.0 g, 0.106 mol) in acetic acid (400 ml), conc. nitric acid (23 ml) was added dropwise and the mixture stirred at room temperature for 1 h, diluted with water (200 ml) and the deposited crude product filtered off, washed thoroughly with water and dried. Crystallization from ethanol afforded 20.6 g (83%) of pure product, m.p. 144°C. ^{1}H NMR (300 MHz, $CDCl_3$), δ: 3.88 (s, OCH_3), 4.02 (s, OCH_3), 6.91 (d, J(6,8)=2.2), 7.08 (dd, J(5,6)=8.8, J(6,8)=2.2), 7.16 (d, J(3,4)=8.8), 7.71 (d, J(5,6=8.8), 7.86 (d, J(3,4)=8.8).

2.2.2. 4-(4-Alkoxybenzoyloxy)benzoic acids (2$_n$). These were obtained according to [30]: 4-(4-hexyloxybenzoyloxy)benzoic acid (**2$_6$**) Cr 130 N 232 I; 4-(4-octyloxybenzoyloxy)benzoic acid (**2$_8$**) Cr 128 SmA 191

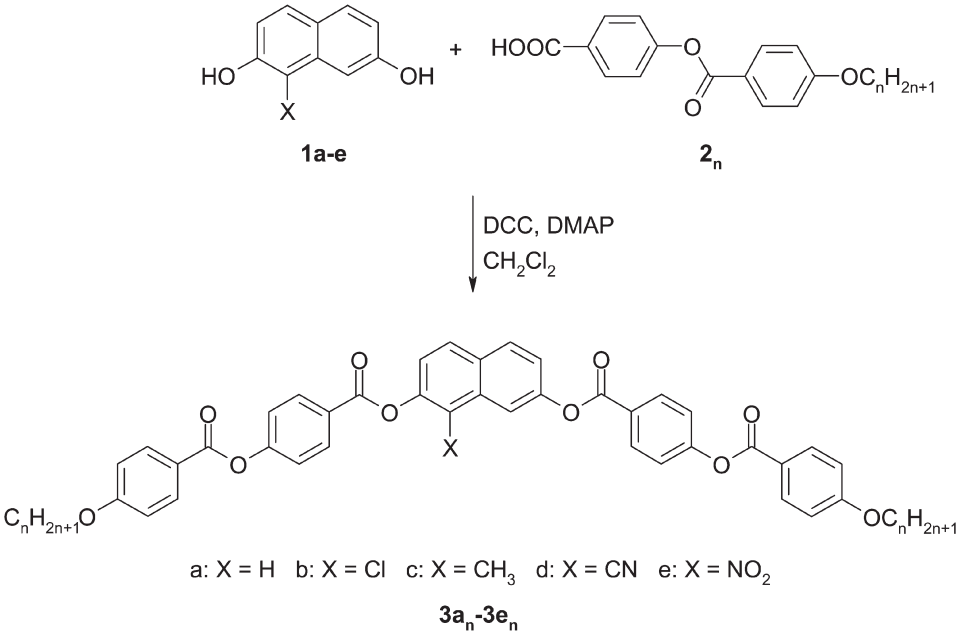

Scheme 1. Synthesis of compounds **3a**$_n$–**3e**$_n$.

N 222 I; 4-(4-decyloxybenzoyloxy)benzoic acid (**2_{10}**) Cr 133 SmA 204 N 218 I; and 4-(4-dodecyloxybenzoyloxy)benzoic acid (**2_{12}**) Cr 120 SmA 182 N 213 I.

2.2.3. 1-Nitronapthalene-2,7-diol (1e). A mixture of 1-nitro-2,7-dimethoxynapthalene (0.30 g, 1.49 mmol) and pyridinium chloride (5.0 g, 0.043 mol) was heated at 170°C for 5 days, cooled to room temperature, dissolved in water (150 ml) and extracted with ethyl acetate (3×100 ml). The combined organic solution was dried with anhydrous $MgSO_4$. After evaporation the crude product was purified by column chromatography (silica gel, elution with toluene/*tert*-butyl methyl ether 25/1) and crystallized from chloroform; 90 mg (40%) of **1e** was obtained, m.p. 202°C. ^{1}H NMR (300 MHz, DMSO-d_6), δ: 6.89 (dd, J(5,6)=8.8, J(6,8)=2.5), 7.00 (d, J(3,4)=8.8), 7.24 (d, J(6,8)=8.8), 7.59 (d, J(5,6=8.8), 7.67 (d, J(3,4)=8.8).

2.2.4. 1-Substituted naphthalene-2,7-diyl bis[4-(4-alkoxybenzoyloxy)benzoate] (3a–e). A mixture of diol **1a**–**e** (10 mmol), acid **2** (25 mmol), DCC (30 mmol), a catalytic amount of DMAP (10 mg) and dry dichloromethane (50 ml) was stirred at room temperature for 1 day; water (0.5 ml) was added and after 30 min the precipitate was filtered off and washed with dichloromethane (20 ml). The filtrate was evaporated to dryness and the crude product purified by column chromatography (silica gel, elution with dichloromethane) and crystallization from toluene and acetone; yields 37–90%. Because of the similarity of homologous compounds, spectral data of materials in the correponding series were identical. Therefore only hexyl derivatives of **$3a_6$**–**$3e_6$** are presented here.

3a: IR (ν, $CHCl_3$, cm^{-1}): 2 933, 2 874, 1 736 (COO), 1 604, 1 580, 1 469, 1 258, 1 161. ^{1}H NMR (300 MHz, $CDCl_3$), δ: 0.92 (t, J=7.4, CH_3), 1.35 (m, $(CH_2)_2$), 1.54 (m, CH_2), 1.86 (t, CH_2), 4.06 (t, CH_2O), 6.99 (d, J=8.8, 4 H), 7.38 (dd, J_1=8.8, J_2=2.2, H-3, H-6), 7.40 (d, 4 H), 7.71 (d, J=2.2, H-1, H-8), 7.95 (d, H-4, H-5), 8.17 (d, 4 H), 8.33 (d, 4 H). Elemental analysis for $C_{50}H_{48}O_{10}$ (808.93): calcd, C 74.24, H 5.98; found, C 74.33, H 5.89%.

3b: IR (ν, $CHCl_3$, cm^{-1}): 2 933, 1 737 (COO), 1 604, 1 512, 1 414, 1 258, 1 161. ^{1}H NMR (300 MHz, $CDCl_3$), δ: 0.92 (t, J=7.4, $2 \times CH_3$), 1.35 (m, $2 \times (CH_2)_2$), 1.49 (m, $2 \times CH_2$), 1.84 (t, $2 \times CH_2$), 4.06 (t, $2 \times CH_2O$), 7.00 (d, 4 H), 7.40 (dd, J_1=9.4, J_2=2.0, H-6), 7.41 (d, 4 H), 7.42 (d, J=9.1, H-3), 7.44 (d, J=2.0, H-8), 7.44 (d, J=8.8, H-4), 7.98 (d, J=9.1, H-5), 8.17 (d, 4 H), 8.38 (m, 4 H). Elemental analysis for $C_{50}H_{47}ClO_{10}$ (843.38): calcd, C 71.21, H 5.62, Cl 4.20; found, C 71.16, H 5.55, Cl 4.03.

3c: IR (ν, $CHCl_3$, cm^{-1}): 2 933, 1 735 (COO), 1 604, 1 512, 1 258, 1 160. ^{1}H NMR (300 MHz, $CDCl_3$), δ: 0.92 (t, J=7.4, $2 \times CH_3$), 1.35 (m, $2 \times (CH_2)_2$), 1.49 (m,

Table 1. Phase transition temperatures, T_{tr}, and corresponding enthalpies, ΔH, measured on cooling from the isotropic phase; m.p. is melting point, X indicates the substituent, B_x indicates the banana mesophase.

Compound	n	X	m.p./°C	ΔH/ kJ mol^{-1}	Cr	T_{tr}/°C	ΔH/kJ mol^{-1}	B_x	T_{tr}/°C	ΔH/ kJ/mol^{-1}	I
$3a_6$	6	H	147	+13.2	•	136	−10.3	B_1	199	−9.9	•
$3a_8$	8		151	+24.7	•	129	−21.8	B_1	182	−18.6	•
$3a_{10}$	10		140	+17.0	•	131	−19.4	B_1	168	−17.4	•
$3a_{12}$	12		135	+15.5	•	122	−10.2	B_N	170	−20.2	•
$3b_6$	6	Cl	145	+33.3	•	115	−15.5	B_1	175	−18.0	•
$3b_8$	8		135	+30.9	•	119	−15.7	B_1	159	−17.8	•
$3b_{10}$	10		125	+32.8	•	115	−21.1	B_1	142	−18.3	•
$3b_{12}$	12		111	+38.3	•	105	−32.3	B_2	140	−20.5	•
$3c_6$	6	CH_3	193	+30.1	•	162	−18.2	B_1	184	−11.9	•
$3c_8$	8		178	+42.0	•	157	−21.4	B_1	168	−21.0	•
$3c_{10}$	10		141	+17.3	•	123	−16.4	B_1	156	−20.2	•
$3c_{12}$	12		135	+21.5	•	116	−19.7	B_2	152	−22.3	•
$3d_6$	6	CN	158	+9.0	•	130	−7.8	B_1	187	−19.1	•
$3d_8$	8		138	+46.2	•	98	−14.5	B_1	173	−21.3	•
$3d_{10}$	10		115	+45.8	•	75	−4.3	B_7	166	−23.6	•
$3d_{12}$	12		77	+29.3	•	74	−6.6	B_7	171	−25.3	•
$3e_6$	6	NO_2	121	+19.0	•	115	−13.8	B_1	169	−18.2	•
$3e_8$	8		135	+33.9	•	115	−1.5	B_1	153	−17.6	•
$3e_{10}$	10		118	+36.5	•	117	−0.8	B_7	143	−21.1	•
$3e_{12}$	12		78	+4.1	•	65	−9.2	B_7	147	−17.2	•

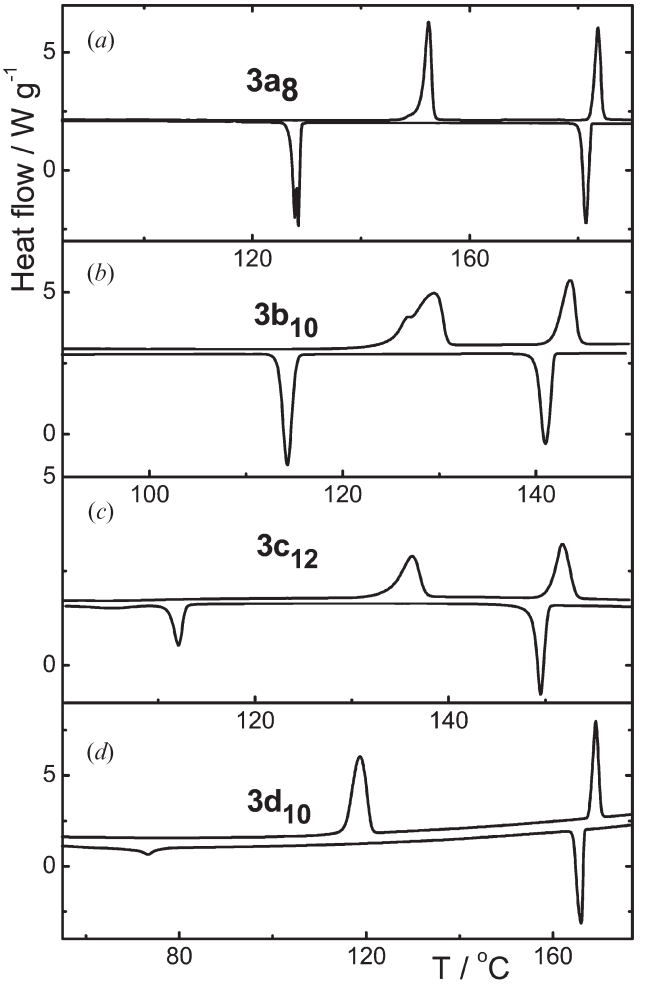

Figure 1. Typical DSC plots for the compounds (*a*) **3a$_8$** (*X*=H), (*b*) **3b$_{10}$** (*X*=Cl), (*c*) **3c$_{12}$** (*X*=CH_3), (*d*) **3d$_{10}$** (*X*=CN). The upper curve shows the second heating run, the lower curve corresponds to the subsequent cooling.

$2\times CH_2$), 1.83 (t, $2\times CH_2$), 2.54 (s, CH_3), 4.06 (t, $2\times CH_2O$), 7.00 (d, 4 H), 7.32 (dd, J_1=9.4, J_2=2.0, H-6), 7.33 (d, J=9.1, H-3), 7.41 (d, 4 H), 7.82 (d, J=9.4, H-5), 7.86 (d, J=2.0, H-8), 7.95 (d, J=9.1, H-4), 8.17 (d, 4 H), 8.36 (m, 4 H). Elemental analysis for $C_{51}H_{50}O_{10}$ (822.96): calcd, C 74.43, H 6.12; found, C 74.31, H 6.01%.

3d: IR (ν, $CHCl_3$, cm^{-1}): 2 933, 1 735 (COO), 1 604, 1 512, 1 258, 1 160. ^{1}H NMR (300 MHz, $CDCl_3$), δ: 0.90 (t, J=7.4, $2\times CH_3$), 1.35 (m, $2\times(CH_2)_2$), 1.48 (m, $2\times CH_2$), 1.83 (t, $2\times CH_2$), 4.06 (t, $2\times CH_2O$), 7.00 (d, 4 H), 7.41 (d, 4 H), 7.57 (dd, J_1=9.4, J_2=2.1, H-6), 7.60 (d, J=9.1, H-3), 8.05 (d, J=9.1, H-4), 8.07 (d, J=2.1, H-8), 8.17 (d, 4 H), 8.19 (d, J=9.4, H-5), 8.36 (m, 4 H). Elemental analysis for $C_{51}H_{47}NO_{10}$: calcd, C 73.45, H 5.68, N 1.68; found, C 73.36, H 5.61, N 1.54%.

3e: IR (ν, $CHCl_3$, cm^{-1}): 2 929, 2 858, 1 739 (COO), 1 603, 1 512, 1 255, 1 159. ^{1}H NMR (300 MHz, $CDCl_3$), δ: 0.90 (t, J=7.4, $2\times CH_3$), 1.35 (m, $2\times(CH_2)_2$), 1.49 (m, $2\times CH_2$), 1.83 (t, $2\times CH_2$), 4.06 (t, $2\times CH_2O$), 7.00 (d, 4 H), 7.41 (d, 4 H), 7.55 (d, J=9.5, H-5), 7.56 (dd, J_1=9.5, J_2=2.0, H-6), 7.82 (d, J=9.5, H-5), 7.88 (d, J=2.0, H-8), 8.05 (d, J=9.1, H-4), 8.17 (d, 4 H), 8.36 (m, 4 H). Elemental analysis for $C_{50}H_{47}NO_{12}$ (853.93): calcd, C 70.33, H 5.55, N 1.64; found, C 70.20, H 5.36, N 1.55%.

3. Results

The phase transition temperatures and associated enthalpy changes are collected in table 1. All the compounds studied exhibit one mesophase. The compounds with short terminal chains exhibit a phase that has the same features irrespective of the type of substitution. This phase is identified as the B_1 phase from texture observation and X-ray data (see later). Increasing of the terminal chain length causes a diversification of phases. The DSC thermograms for selected compounds are shown in figure 1. The mesophases may be undercooled typically by 15 to 20 K. In the case of **3a$_8$** the crystallization peak is split and for **3a$_{10}$** there is one additional peak below the crystallization, indicating a phase transition in the solid state. The identification of phases and their properties are described next in more detail.

For non-substituted compounds, **3a$_n$** with short aliphatic chains up to n=10, the rectangular columnar B_1 phase was observed. The planar texture of the B_1 phase exhibits mosaic non-switchable domains. The X-ray diffraction, pattern of a non-oriented sample of **3a$_6$** exhibits several reflections in the small angle region and diffuse scattering around $2\Theta\sim20^\circ$. The reflection could be indexed on the basis of a rectangular centred lattice with parameters a=4.18 nm and b=3.12 nm. The texture of the mesophase shown by **3a$_8$** and **3a$_{10}$** exhibits the same features. For **3a$_{12}$** another mesophase appears; its planar texture shows large dark domains distinguishable under the rotation of the polarizer from the crossed position (see figure 2). The domains do not change under an electric field up to 50 V μm^{-1} and the polarization current exhibits no switching. Free-standing films show slightly birefringent domains with diffuse boundaries (see figure 3). The contrast between domains grows and is interchanged when rotating the polarizer clockwise or anticlockwise from the crossed position.

The X-ray pattern indicates a layered structure (layer thickness is about 3.9 nm, see table 2). The corresponding reflection is wider than usual layer reflections, which may indicate a defect in the layer structure or a large period undulation. Such an undulation would produce a weak reflection, and if coinciding with the main layer

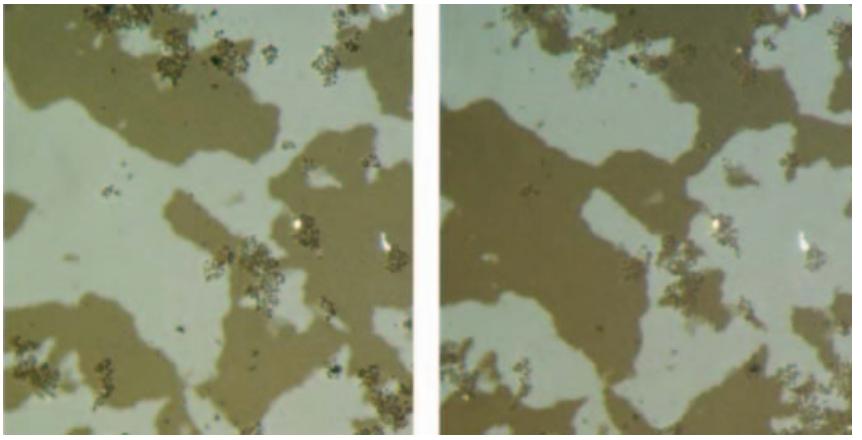

Figure 2. The texture of **3a$_{12}$** (X=H) observed in the B_N phase at T=160°C on a planar 6 µm cell. The two photos differ in the sense of rotation of the polarizer and analyser (7° clockwise and anticlockwise from crossed polarizer directions, which are parallel to the edges of the picture). Picture width is about 150 µm.

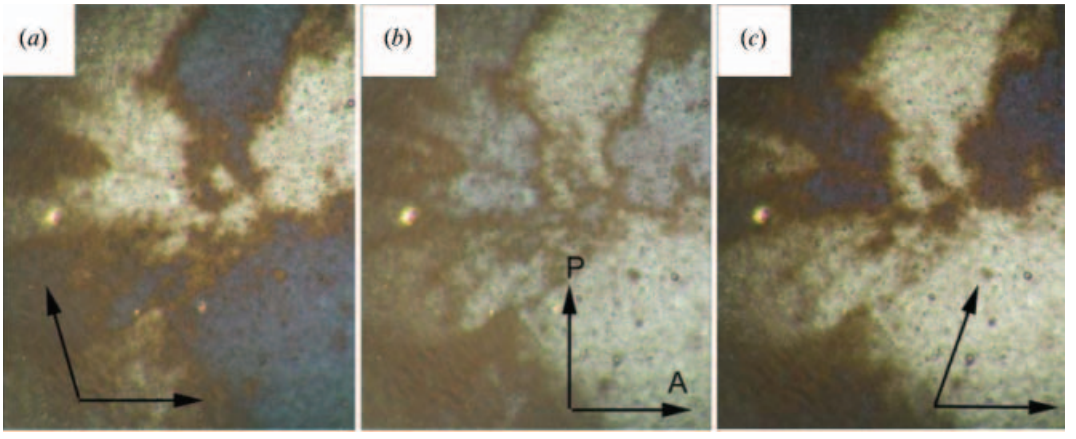

Figure 3. Texture of the free-standing film for **3a$_{12}$** (X=H) observed in the B_N phase at T=157°C. The polarizer is crossed by an angle of about 6° (*a*) clockwise or (*c*) anticlockwise from (*b*) the crossed position. Picture width is about 150 µm.

reflection could cause its widening. The wide angle region exhibits a diffuse diffraction maximum, showing structural disorder within layers. Contact samples were prepared from **3a$_{12}$** with **3c$_{12}$** and with **3d$_{12}$** which exhibit the B_2 phase and the B_7 phase respectively in the same temperature range (see table 1). Both contact samples showed non-miscibility of the phases in contact. No miscibility was achieved, even though the contact samples were preheated to the isotropic phase. The identification of the mesophase for non-substituted **3a$_{12}$** is ambiguous and hence we denote this mesophase as the B_N phase.

In Cl-substituted compounds, **3b$_n$**, the B_1 phase exists for n=6, 8 and 10. Compound **3b$_{12}$** exhibits the B_2 phase. The growth of the B_2 phase from the isotropic is accompanied by specific features—see dendritic-like nuclei in figure 4 (*a*). The texture of the B_2 phase is rather fine and the intensity of transmitted light grows under a d.c. field. The transmittance is proportional to the applied d.c. field up to about 20 V µm^{-1}. In figure 4 (*b*) it is possible clearly to distinguish the edge of an sample covered with electrode. The bright upper part is under the d.c. field and the dark lower part of the sample is not covered by the electrode. The application

Table 2. Layer spacing d, length of molecules L, and tilt angle of compounds containing long chains.

Compound	Phase	d/nm	L/nm	tilt angle/°
3a$_{12}$	B_N	3.9	5.3	43
3b$_{12}$	B_2	3.9	5.3	43
3c$_{12}$	B_2	3.9	5.3	43
3d$_{10}$	B_7	3.6	4.9	43
3d$_{12}$	B_7	3.7	5.3	46

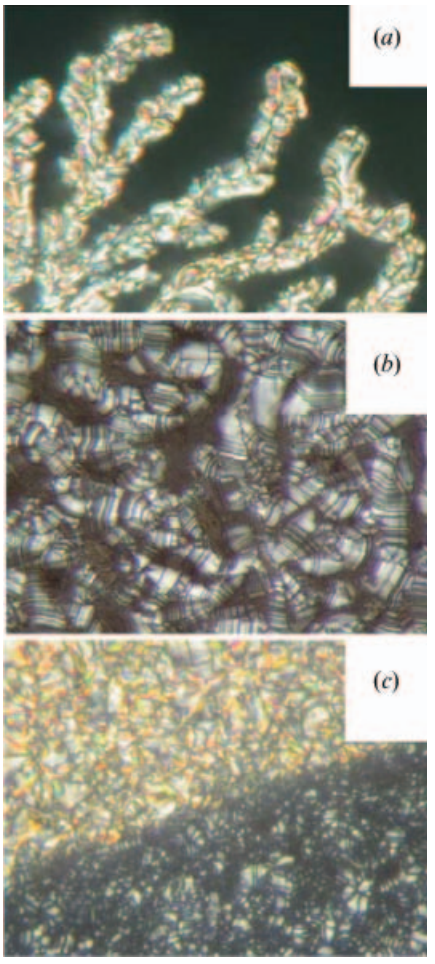

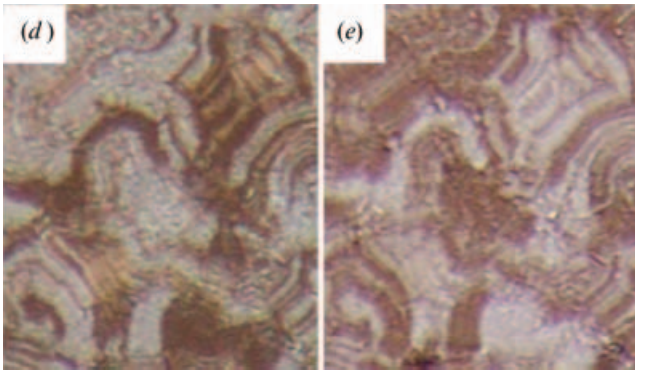

Figure 4. Planar textures of **3b$_{12}$** (X=Cl). (*a*) The phase transition from isotropic to the B_2 phase at T=144°C, (*b*) with a d.c. electric field 10 V μm^{-1} in the vicinity of the edge of the electrode which is in the upper part of the picture and (*c*) under a slow (3 Hz) a.c. electric field 20 V μm^{-1}. Width of every photomicrograph is about 120 μm. In (*d*)/(*e*) the a.c. electric field is switched off and the polarizer rotated clockwise/anticlockwise by 7° from crossed position. Width of (*d*), (*e*) pictures is about 200 μm.

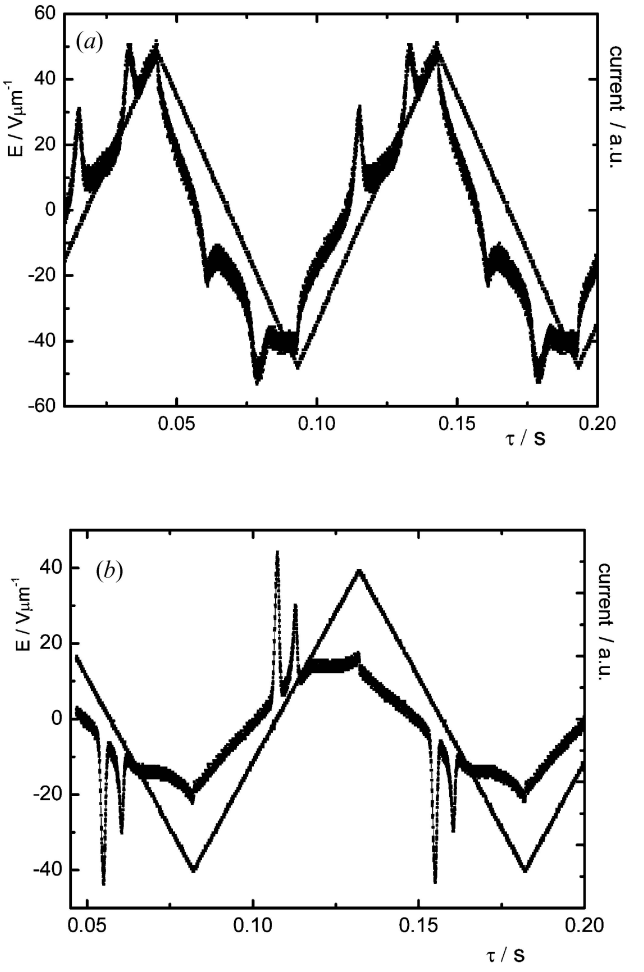

Figure 5. The profile of the polarization current for (*a*) **3b$_{12}$** taken at T=125°C, and (*b*) **3c$_{12}$** at T=132°C, frequency 12 Hz.

of an a.c. electric field leads to the formation of a stripe texture, figure 4 (*c*). After switching off the a.c. field, the texture relaxes into a dark state with domains, which become alternately brighter and darker on clockwise or anticlockwise rotation of the polarizer by a small angle from the crossed position. This indicates that the domains rotate the polarization of light in the opposite sense, see figures 4 (*d*) and 4 (*e*).

The profile of the switching current exhibits two peaks in the B_2 phase of **3b$_{12}$** for a low frequency a.c. field, which provides evidence of the antiferroelectric character of this phase, see figure 5 (*a*). In the dielectric spectroscopy study, a single mode is observed in the B_2 phase with a relaxation frequency of hundreds of kHz, which slightly decreases with decreasing temperature, see figure 6 (*a*). This mode is weak and completely disappears in the isotropic as well as in the crystalline phases. This fact indicates the collective character of this mode.

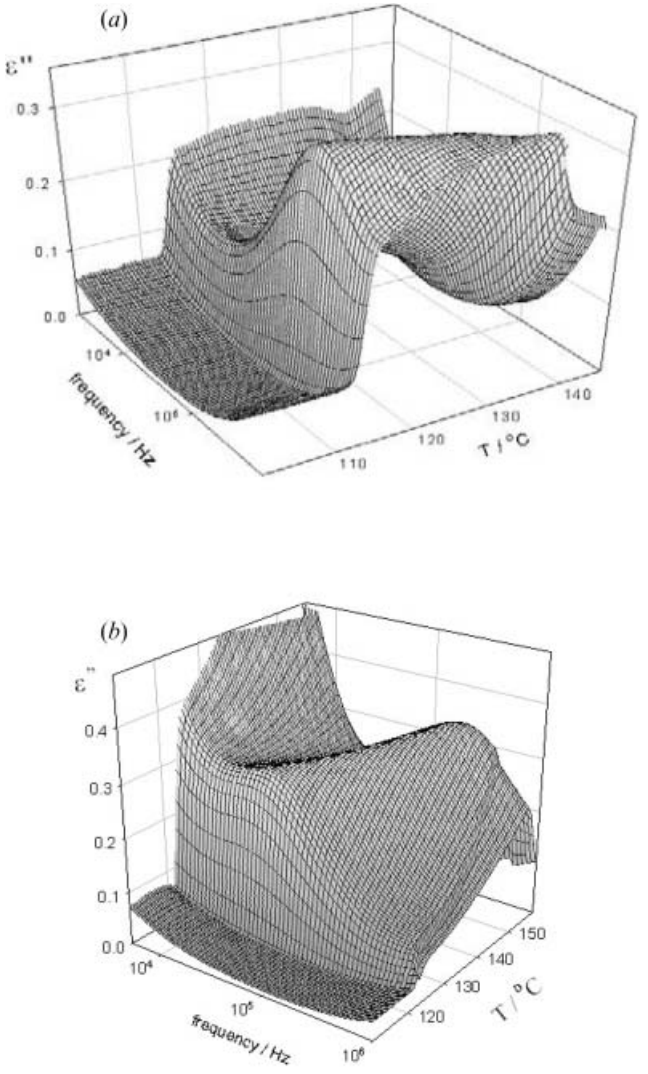

Figure 6. 3-D temperature–frequency plots of the imaginary part of dielectric permittivity ε'' for (*a*) **3b$_{12}$** and (*b*) **3c$_{12}$**.

X-ray measurements were made in the B_2 phase on non-oriented samples. The diffraction pattern exhibits sharp small angle reflections corresponding to the smectic layers; the calculated layer spacing is shown in table 2. In the wide angle region a diffuse diffraction maximum occurs, indicating a liquid-like order within layers.

In methyl-substituted compounds, **3c$_n$**, the B_1 phase again occurs for $n=6$, 8 and 10. In **3c$_8$** the B_1 phase was studied in more detail. Typical mosaic texture of the B_1 phase is shown in figure 7 for a 6 μm planar sample. The X-ray diffraction pattern of a non-oriented sample exhibits a broad diffuse peak at large angles and several reflections in the small angle region. The indexed reflections suggest a rectangular centred lattice with parameters $a=4.53$ nm and $b=3.45$ nm. The lattice type was proved by the pattern of an oriented sample. The reciprocal lattice is sketched together with the Miller indices of the observed reflection in figure 8 (*a*). In addition, the pattern indicates that the molecules are aligned parallel to the *a*-axis of the lattice.

The B_2 phase was observed in compound **3c$_{12}$**. During the transition from the isotropic phase, this phase grows in the form of leaf-like nuclei, figure 9 (*a*), with the extinction position inclined from the axes of the crossed polarizers. Under an electric field applied at about $10\,V\,\mu m^{-1}$ for several minutes, the virgin coloured texture transforms into the typical fan-shaped texture. In zero electric field, figure 9 (*b*), the fans are dark, which indicates low birefringence, and have the extinction parallel to the crossed polarizers direction. Under a d.c. electric field the birefringence grows significantly and extinction brushes rotate by an angle of about 45° clockwise or anticlockwise, respective to the polarity, see figure 9 (*c*). After switching off the field, the dark texture with the extinction parallel to the crossed polarizers direction is restored, figure 9 (*b*). The virgin texture, 9 (*a*), may be restored only by heating into the isotropic phase with subsequent cooling. A switching current profile with two peaks provides evidence about the antiferroelectric character of the B_2 phase, see figure 5 (*b*). A single relaxation mode is detected in the dielectric spectroscopy in this phase, figure 6 (*b*). Its dielectric strength $\Delta\varepsilon\approx0.4$ and relaxation frequency decreases (350–30 kHz) on cooling. For **3c$_{12}$** the X-ray pattern, figure 8 (*b*), gives the layer spacing 3.9 nm. This value combined with CPK simulations of the length of the molecule, results in a tilt angle of about 43° (table 2).

For the cyano- and nitro-substituted compounds with $n=6$ and 8, the B_1 phase has been found. The mesophase of compounds with $n=10$ and 12 exhibits a typical texture of the B_7 phase for both series. Irregular spiral nuclei and straight lancet-like germs arise on cooling from the isotropic phase (see figure 10). Free-standing films form a fingerprint texture (see figure 11) similar to that observed in the B_7 phase for another compound [31]. X-ray diffraction studies were performed for **3d$_{10}$** and **3d$_{12}$** in the B_7 phase. The diffraction pattern consists of the layer reflection, followed by a satellite, which that the smectic layers are undulated. The position of the satellite determines the period of undulation within 9–10 nm.

4. Discussion and conclusions

We have prepared 20 new compounds derived from 1-substituted naphthalene-2,7-diol, and each of them exhibits one mesophase. In materials with shorter alkyl chains ($n=6$, 8 and 10 for H, Cl and CH_3; $n=6$ and 8 for CN and NO_2 substituted compounds) the B_1 phase has

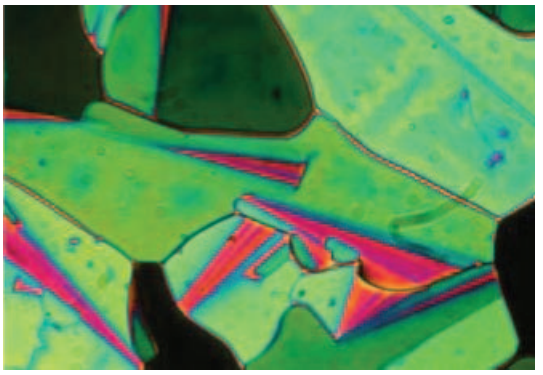

Figure 7. The planar texture of the B_1 phase observed for **3c$_8$** at $T=162^{\circ}C$. Picture width is about 350 µm.

been established. X-ray studies enabled us to determine the dimension of its rectangular centred lattice. To create a structural model of the B_1 phase it has been necessary to estimate the molecular length. Depending on the assumed molecular shape, different values of the length of molecule could be obtained. We mainly used CPK models, figure 12 (*a*), which gives a length of the **3c$_8$** molecule to be approximately 4.4 nm. The structural

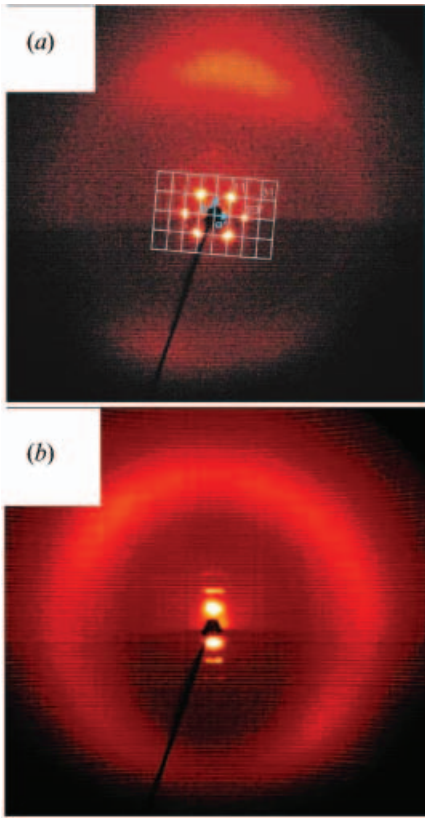

Figure 8. X-ray pattern for (*a*) **3c$_8$** taken at $T=160^{\circ}C$ in the B_1 phase, (*b*) **3c$_{12}$** taken at $T=145^{\circ}C$ in the B_2 phase.

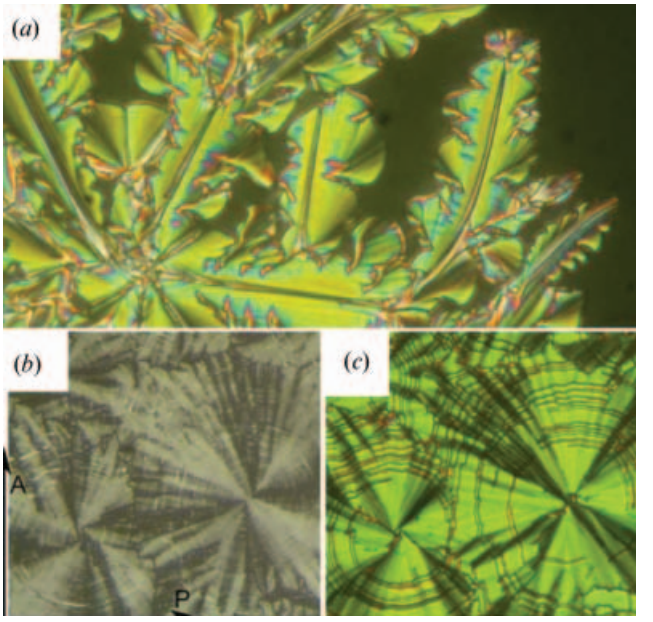

Figure 9. Planar textures of **3c$_{12}$** ($X=CH_3$). (*a*) Growth of the B_2 phase from the isotropic phase. The SmC_AP_A texture (*b*) without field and (*c*) under a d.c. electric field of 20 V µm^{-1}. (*b*) and (*c*) were observed at $T=140^{\circ}C$; the width of (*b*) and (*c*) is about 200 µm. Direction of polarizer and analyser is parallel to the edge of all photomicrographs.

model derived on the basis of this length is shown in figure 12 (*b*).

The mesophase denoted as B_N in the non-substituted compound with $n=12$ exhibits domains rotating polarized light in both planar and free-standing samples. No polarization switching has been found up to the field 50 V µm^{-1}. X-ray study shows a broad reflection from the smectic layers and liquid-like order within the layers. The behaviour of this phase is similar to that of the high temperature phase, which has been reported as

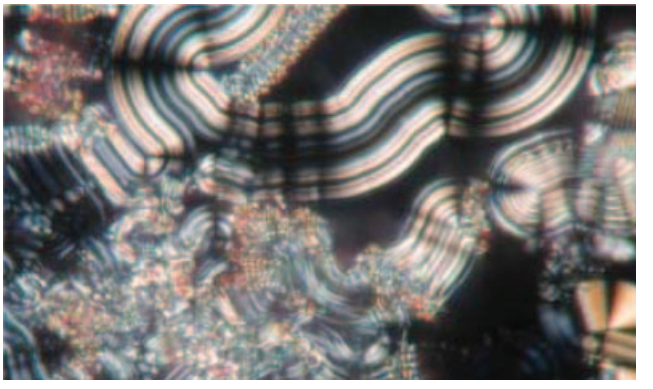

Figure 10. Texture of **3d$_{10}$** ($X=CN$) at the phase transition from the isotropic to the B_2 phase for a planar 6 µm cell. Picture width is about 350 µm.

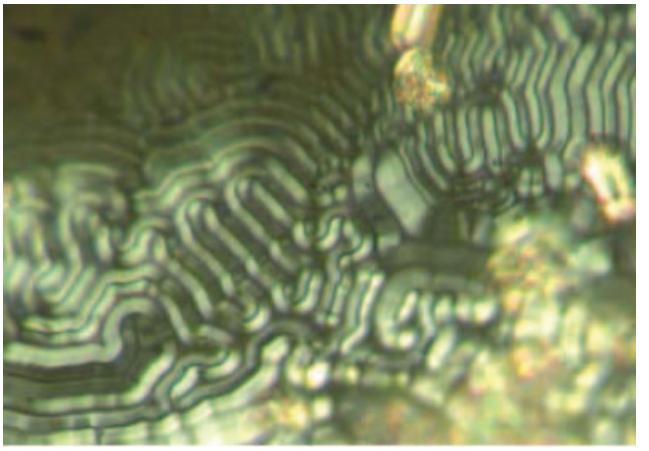

Figure 11. Free-standing film for **3e$_{12}$** (X=NO_2) taken in the B_7 phase at T=137°C. Picture width is about 150 µm.

SmX [32]. Later detailed synchrotron study of the SmX phase disclosed satellites behind the layer diffraction, which assigned the SmX phase as the B_7 phase [33]. Microscope studies have shown texture differences between the SmX phase [32] and the B_N phase. The SmX phase exhibited wound chains typical for the B_7 phase, which have never been observed for the B_N phase reported here. Free-standing films of the B_N phase showed specific features not yet reported in the literature. Moreover, in **3a$_{12}$** our study of contact samples has excluded not only the occurrence of the B_2 phase, but also the B_7 phase (contact probe with compound **3d$_{12}$**, which exhibits the B_7 phase). Thus, an unambiguous identification of the B_N phase structure will require further investigation.

It is important to note that the non-substituted materials denoted here as **3a**, with 7, 8, and 9 carbon atoms in the alkyl chain have been described earlier, but their mesophases were not characterized [3]. Later the series was extended with materials with n=4, 11 and 16 [25]. In agreement with our present results it was shown that the substances with the short alkyl chains generally exhibited the columnar B_1 phase. However, for materials with n=11 and 16 the SmC_AP_A mesophase was reported [25]. Let us emphasize that in the study reported here the B_2 phase is unambiguously excluded for n=12 (compound **3a$_{12}$**).

The B_2 phases in the Cl- and CH_3-substituted compounds with n=12 are antiferroelectric. For the latter, the chiral SmC_AP_A structure is confirmed by the changes of texture under the field (see figure 9). For all compounds studied the measured layer spacing is considerably smaller than the calculated molecular length. This proves the tilted arrangement of molecules within layers; the tilt angle could be estimated as approximately 43°–46° (see table 2). For compound

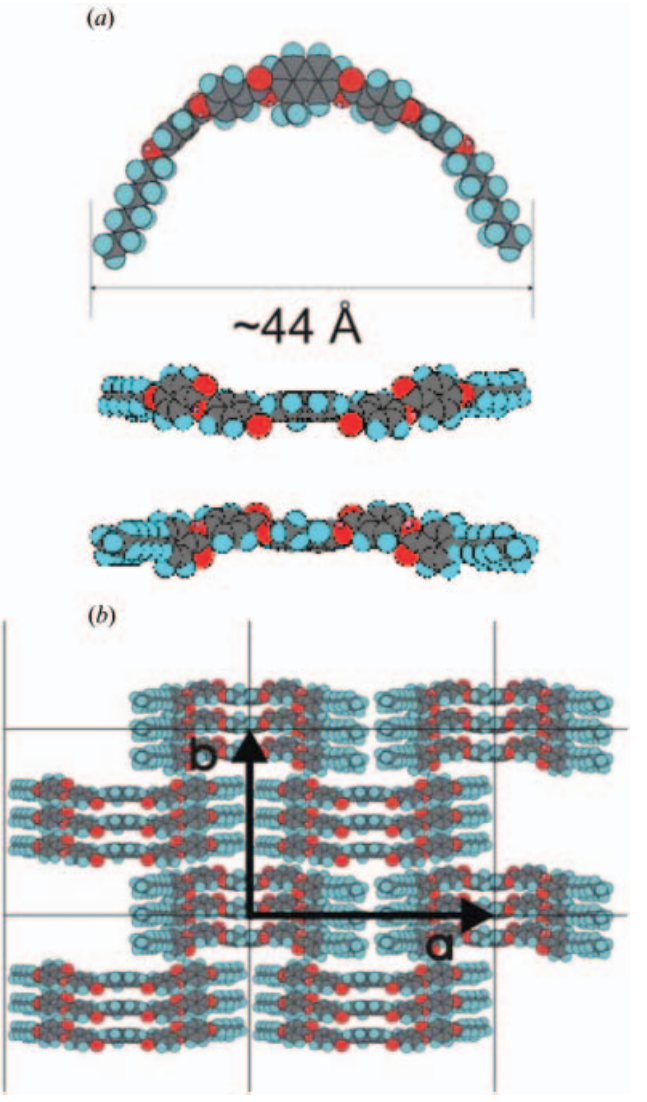

Figure 12. (*a*) Profile of the **3c$_8$** molecule obtained on the basis of CPK molecular simulations. (*b*) Model of the B_1 phase of **3c$_8$** derived from the X-ray data.

3c$_{12}$ this value fits to the angle of rotation of extinction brushes from crossed position in a planar cell under an electric field, see figure 9 (*c*).

In CN- and NO_2-substituted compounds with n=10 and 12, a typical B_7 phase occurs with the period of layer undulation of about 10 nm established by the X-ray study. The existence of the B_7 phase is confirmed by the texture in both planar and free-standing samples. The phases in compounds with long chains (B_N, B_2, and B_7) are tilted. The tilt angle is estimated from a comparison of the molecular length and the layer spacing (see table 2). In the CH_3-substituted compounds that value is in accord with the observation of the optical extinction under the field.

Comparing the results with the earlier studied series of related Schiff's bases [27], replacement of the imine moiety leads to a significant drop of clearing temperature in all the series of compounds **3a**–**3e** studied. On the other hand, the introduction of another ester linking group leads to a partial loss of variety of the mesophases formed. Compounds with shorter alkyl chains tend to form the columnar B_1 phase. The type of the lateral substituent strongly influences the formation of the corresponding type of B phase. While methyl and chloro substitution in the core supports formation of the SmC_AP_A phase, the strongly polar cyano and nitro groups lead to the appearance of the B_7 phase. The B_7 phase described here has an undulated structure, similar to that of phases described previously [31, 33].

Acknowledgements

This work was supported by the Grant Agency of the Czech Republic (Project Nos 202/02/0840 and 202/05/0431), Ministry of Education, Youth and Sports of the Czech Republic (project Nos OCD14.60 and AVOZ1-010-914), and European Project COST D14 WG 00015.

References

[1] T. Niori, T. Sekine, J. Watanabe, T. Furukawa, H. Takezoe. *J. mater. Chem.*, **6**, 1231 (1996).
[2] G. Pelzl, S. Diele, S. Grande, A. Jákli, C. Lischka, H. Kresse, H. Schmalfuss, I. Wirth, W. Weisslfog. *Liq. Cryst.*, **26**, 401 (1999).
[3] G. Pelzl, S. Diele, W. Weissflog. *Adv. Mater.*, **11**, 707 (1999).
[4] D. Shen, A. Pegenau, S. Diele, I. Wirth, C. Tschierske. *J. Am. chem. Soc.*, **122**, 1593 (2000).
[5] J. Thisayukta, Y. Nakayama, J. Watanabe. *Liq. Cryst.*, **27**, 1129 (2000).
[6] J.P. Bedel, J.C. Rouillon, J.P. Marcerou, M. Laguerre, H.T. Nguyen, M.F. Achard. *Liq. Cryst.*, **28**, 1285 (2001).
[7] M. Hird, J.W. Goodby, N. Gough, K.J. Toyne. *J. mater. Chem.*, **11**, 2732 (2001).
[8] B.K. Sadashiva, N. Shreenivasa Murthy, S. Dhara. *Liq. Cryst.*, **28**, 483 (2001).
[9] I. Wirth, S. Diele, A. Eremin, G. Pelzl, S. Grande, L. Kovalenko, N. Pancenko, W. Weissflog. *J. mater. Chem.*, **11**, 1642 (2001).
[10] J.C. Rouillon, J.P. Marcerou, M. Laguerre, H.T. Nguyen, M.F. Achard. *J. mater. Chem.*, **11**, 2946 (2001).
[11] H. Nádasi, W. Weissflog, A. Eremin, G. Pelzl, S. Diele, B. Das, S. Grande. *J. mater. Chem.*, **12**, 1316 (2002).
[12] W. Weissflog, H. Nádasi, U. Dunemann, G. Pelzl, S. Diele, A. Eremin, H. Kresse. *J. mater. Chem.*, **11**, 2748 (2001).
[13] J.P. Bedel, J.C. Rouillon, J.P. Marcerou, M. Laguerre, H.T. Nguyen, M.F. Achard. *J. mater. Chem.*, **12**, 2214 (2002).
[14] M. Kašpar, V. Hamplová, V. Novotná, M. Glogarová, P. Vaněk. *J. mater. Chem.*, **12**, 2221 (2002).
[15] H.N. Shreenivasa Murthy, B.K. Sadashiva. *Liq. Cryst.*, **30**, 1051 (2003).
[16] V. Prasad, S.-W. Kang, S. Kumar. *J. mater. Chem.*, **13**, 1259 (2003).
[17] H.N. Shreenivasa Murthy, B.K. Sadashiva. *J. mater. Chem.*, **13**, 2863 (2003).
[18] R. Amarantha Reddy, B.K. Sadashiva. *Liq. Cryst.*, **30**, 1031 (2003).
[19] J. Mieczkowski, K. Gomola, K. Koseska, D. Pociecha, J. Szydlowska, E. Gorecka. *J. mater. Chem.*, **13**, 2132 (2003).
[20] H.N. Shreenivasa Murthy, B.K. Sadashiva. *Liq. Cryst.*, **31**, 361 (2004).
[21] K. Kumazawa, M. Nakata, F. Araoka, Y. Takanishi, K. Ishikawa, J. Watanabe, H. Takezoe. *J. mater. Chem.*, **14**, 157 (2004).
[22] J. Thisayukta, Y. Nakayama, S. Kawauchi, H. Takezoe, J. Watanabe. *J. Am. chem. Soc.*, **122**, 7441 (2000).
[23] R. Amarantha Reddy, B.K. Sadashiva. *Liq. Cryst.*, **27**, 1613 (2000).
[24] B.K. Sadashiva, H.N. Shreenivasa Murthy, S. Dhara. *Chem. Commun.*, 1972 (2001).
[25] R. Amarantha Reddy, B.K. Sadashiva. *J. mater. Chem.*, **14**, 1936 (2004).
[26] H.N. Shreenivasa Murthy, B.K. Sadashiva. *Liq. Cryst.*, **31**, 1347 (2004).
[27] J. Svoboda, V. Novotná, V. Kozmík, M. Glogarová, W. Weissflog, S. Diele, G. Pelzl. *J. mater. Chem.*, **13**, 2104 (2003).
[28] O. Fischer, W. Kern. *J. prakt. Chem.*, **94**, 44 (1916).
[29] M. Janczewski, B. Florkiewicz. *Rocz. Chem.*, **35**, 953 (1961).
[30] S.M. Kelly, R. Buchecher. *Helv. chim. Acta.*, **71**, 461 (1988).
[31] G. Pelzl, M.W. Schröder, U. Dunemann, S. Diele, W. Weissflog, C. Jones, D. Coleman, N.A. Clark, R. Stannarius, J. Li, B. Das, S. Grande. *J. mater. Chem.*, **14**, 2492 (2004).
[32] A. Eremin, S. Diele, G. Pelzl, H. Nádasi, W. Weissflog. *Phys. Rev. E*, **67**, 021702 (2003).
[33] D.A. Coleman, J. Fernsler, N. Chattham, M. Nakata, Z. Takanishi, E. Körblova, D.R. Link, R.-F. Shao, W.G. Jang, J.E. Maclennan, O. Mondain-Monval, C. Boyer, W. Weissflog, G. Pelzl, L.-C. Chien, J. Zasadzinski, J. Watanabe, D.M. Walba, H. Takezoe, N.A. Clark. *Science*, **301**, 1204 (2003).